



OPEN

Thermal prediction of turbulent forced convection of nanofluid using computational fluid dynamics coupled genetic algorithm with fuzzy interface system

Meisam Babanezhad^{1,2,3}, Iman Behroyan^{4,5}, Ali Taghvaie Nakhjiri⁶, Mashallah Rezakazemi⁷, Azam Marjani^{8,9}✉ & Saeed Shirazian¹⁰

Computational fluid dynamics (CFD) simulating is a useful methodology for reduction of experiments and their associated costs. Although the CFD could predict all hydro-thermal parameters of fluid flows, the connections between such parameters with each other are impossible using this approach. Machine learning by the artificial intelligence (AI) algorithm has already shown the ability to intelligently record engineering data. However, there are no studies available to deeply investigate the implicit connections between the variables resulted from the CFD. The present investigation tries to conduct cooperation between the mechanistic CFD and the artificial algorithm. The genetic algorithm is combined with the fuzzy interface system (GAFIS). Turbulent forced convection of Al₂O₃/water nanofluid in a heated tube is simulated for inlet temperatures (i.e., 305, 310, 315, and 320 K). GAFIS learns nodes coordinates of the fluid, the inlet temperatures, and turbulent kinetic energy (TKE) as inputs. The fluid temperature is learned as output. The number of inputs, population size, and the component are checked for the best intelligence. Finally, at the best intelligence, a formula is developed to make a relationship between the output (i.e. nanofluid temperatures) and inputs (the coordinates of the nodes of the nanofluid, inlet temperature, and TKE). The results revealed that the GAFIS intelligence reaches the highest level when the input number, the population size, and the exponent are 5, 30, and 3, respectively. Adding the turbulent kinetic energy as the fifth input, the regression value increases from 0.95 to 0.98. This means that by considering the turbulent kinetic energy the GAFIS reaches a higher level of intelligence by distinguishing the more difference between the learned data. The CFD and GAFIS predicted the same values of the nanofluid temperature.

Roman symbols

C_p	Specific heat capacity at constant pressure (J/kg K)
d_s	Nanoparticle diameter (m)
d_{water}	Water molecular diameter (m)
k	Thermal conductivity (W/m K)
k_{turb}	Turbulent conductivity (W/m K)
k	Turbulence kinetic energy (m^2/s^2)

¹Institute of Research and Development, Duy Tan University, 550000 Da Nang, Vietnam. ²Faculty of Electrical-Electronic Engineering, Duy Tan University, 550000 Da Nang, Vietnam. ³Department of Artificial Intelligence, Shunderman Industrial Strategy Co., Tehran, Iran. ⁴Faculty of Mechanical and Energy Engineering, Shahid Beheshti University, Tehran, Iran. ⁵Department of Computational Fluid Dynamics, Shunderman Industrial Strategy Co., Tehran, Iran. ⁶Department of Petroleum and Chemical Engineering, Science and Research Branch, Islamic Azad University, Tehran, Iran. ⁷Faculty of Chemical and Materials Engineering, Shahrood University of Technology, Shahrood, Iran. ⁸Department for Management of Science and Technology Development, Ton Duc Thang University, Ho Chi Minh City, Vietnam. ⁹Faculty of Applied Sciences, Ton Duc Thang University, Ho Chi Minh City, Vietnam. ¹⁰Laboratory of Computational Modeling of Drugs, South Ural State University, 76 Lenin prospekt, 454080 Chelyabinsk, Russia. ✉email: azam.marjani@tdtu.edu.vn

p	Static pressure (N/m ²)
Pr	Prandtl number
R	Correlation coefficient or regression number
Re	Reynolds number
T	Temperature (K)
U	Velocity (m/s)

Greek letters

ε	Dissipation rate of turbulence kinetic energy (m ² /s ³)
μ	Dynamic viscosity (kg/m s)
μ_{turb}	Turbulent viscosity (kg/m s)
ρ	Density (kg/m ³)
\varnothing	Particle volume fraction

Subscriptions

eff	Population size
s	Population size

Abbreviations

GA	Genetic algorithm
FIS	Fuzzy inference system
TKE	Turbulent kinetic energy
FCM	Fuzzy c-mean
PS	Population size

Recently, an attempt has been made to improve the efficiency of heat transfer fluids by adding inert solid particles (e.g. alumina) to the fluid for heat transfer applications. If the added particles are at nano size, the fluid can be recognized as nanofluid. These nanofluids are novel heat transfer fluids that are made by dispersion of particles in nanometer sizes in a base working fluid such as refrigerants, oil, water, etc. Utilizing the metallic nanoparticle suspension (such as copper, silver, silicon, and aluminum) has shown more augmentation of the nanofluid conductivity than their conventional base fluids^{1–4}. So, the nanofluids have made a promising area for increasing the heat transfer efficiency in many kinds of applications. Comparing micro- and milli- sized particles, the suspension of the nanoparticles could minimize the drawback of clogging⁵.

The mentioned advantages of the nanofluids as working fluids took the attention of researchers and as a result, a progressive trend has been made in heat transfer investigations for nanofluids both experimentally and computationally as well. The numerical study conducted in⁶ deals with assessing the thermal and hydrodynamic behaviors of completely established turbulent flow of alumina + water nanofluids. Behroyan et al.^{7,8} analyzed the importance of the single and two-phase modeling on the numerical investigations of the nanofluid convective flows. They reported that the single-phase model could be considered for modeling the nanofluid flow if the thermos-physical properties of the nanofluid are adopted precisely. Bahmani et al.⁹ have modeled the heat transfer of the turbulent flow of a nanofluid in a heat exchanger. The increase of the outlet and the wall temperatures by the nanoparticle volume fraction was reported in their study. Bianco et al.¹⁰ numerically simulated and reported the laminar convection of the alumina water based nanofluid in a channel with a rectangular cross-section. It was reported that using the nanofluid, the wall of the channel is cooler than that of using the base fluid. However, the nanofluids impose more pumping power as a result of the more pressure drop than water. Benkhedda et al.¹¹ reported the influence of solid particles shape on heat transfer efficiency as well as pressure loss. According to the results, the most rate of heat transfer was related to the nanoparticle in the blade shape, while the maximum pressure drop is for the shape of the platelet. Sharma et al.¹² highlighted the importance of the nanoparticle material and the base fluid properties on heat transfer efficiency. Zainon and Azmi¹³ reported the heat transfer improvement for the suspension of the hybrid nanoparticles in the mixture of water and Bio-Glycol.

Computational fluid dynamics (CFD) is known as a precise and reputable approach in engineering design and troubleshooting purposes. The predicted thermal and hydrodynamic parameters of fluid flows could help engineers and researchers in the trial and error expenses of the experiments. Although the CFD could predict all variables of the fluid flow, the connections between such variables with each other could not be found by this approach. There are some fluid flow variables related to each other implicitly and the mathematical equations or functions for connecting them cannot be achieved easily. In this case, the machine learning technique of the artificial intelligence (AI) algorithm is a way for finding the data patterns and their changes. The AI algorithms cannot reach the maximum intelligence level (the best intelligence) unless the connections of all learned data are found from each other, and the optimum structure needs to be specified. Although the AI algorithms have been used for data analysis for years in different concepts^{14–21}, a few studies have recently shown the application of the artificial intelligence algorithms in simplification of the CFD modeling^{22–29}. The critical literature review on numerical simulating nanofluid flows shows a deep gap in the applications of artificial intelligence in combination of CFD modeling to establish hybrid simulation methodology. The most studies are simple presentations of the AI algorithm of the adaptive network-based fuzzy interface system (ANFIS) for CFD data capture dealing with fluid flow and transport phenomena³⁰.

For addressing such a research gap, this study reports a novel methodology on the CFD simulating of nanofluid flowing in a heated pipe at turbulent regime. The genetic algorithm based fuzzy interface system, known as GAFIS, is used to learn the CFD results. This investigation tries to develop a correlation relating the temperature distribution of the nanofluid flow to fluid flow nodes position, the inlet temperature, and the turbulent kinetic energy using the GAFIS artificial intelligence. This approach would be a sample idea for finding the implicit function between the fluid flow variables.

Methodology

CFD approach. In the current work, a cylindrical tube is taken into account in a horizontal position ($L = 1$ m and $DI = 0.01$ m). Constant heat flux (85 kW/m^2) is used for the tube wall. The inlet velocity of the nanofluid is 0.91 m/s, while the inlet temperature changes by different values of $300, 305, 310, 315,$ and 320 K. The main equations used here are^{7,31,32}:

Continuity equation:

$$\nabla \cdot (\rho_{eff} \vec{U}) = 0. \quad (1)$$

Momentum equation:

$$\nabla \cdot (\rho_{eff} \vec{U} \vec{U}) = -\nabla P + \nabla \cdot (\mu_{eff} \nabla \vec{U} - \rho_{eff} \overline{UU}). \quad (2)$$

Energy equation:

$$\nabla \cdot (\rho_{eff} C_{p,eff} \vec{U} T) = \nabla \cdot ((k_{eff} + k_{turb}) \nabla T). \quad (3)$$

The relevant equations for the $k - \varepsilon$ turbulence model is written as^{7,31,33,34,30}:

$$\nabla \cdot (\rho_{eff} KU) = \nabla \cdot \left[\left(\frac{\mu_t}{\sigma_k} \right) \nabla (K) \right] + G_k - \rho_{eff} \varepsilon, \quad (4)$$

$$\nabla \cdot (\rho_{eff} \varepsilon U) = \nabla \cdot \left[\frac{\mu_{turb}}{\sigma_\varepsilon} \nabla \varepsilon \right] + \frac{\varepsilon}{k} (C_{1\varepsilon} G_k - C_{2\varepsilon} \rho_{eff} \varepsilon), \quad (5)$$

$$G_k = \mu_{turb} (\nabla U + (\nabla U)^{turb}), \quad \mu_{turb} = \rho_{eff} C_\mu \frac{K^2}{\varepsilon}, \quad (6)$$

$$C_\mu = 0.09, \sigma_k = 1.00, \sigma_\varepsilon = 1.30, C_{1\varepsilon} = 1.44, C_{2\varepsilon} = 1.92$$

The temperature-dependent correlations for water properties are given as follows^{35,29}:

Density³⁶:

$$\rho_{water} = 2446 - 20.674T + 0.11576T^2 - 3.12895 \times 10^{-4}T^3 + 4.0505 \times 10^{-7}T^4 - 2.0546 \times 10^{-10}T^5, \quad (7)$$

Viscosity³⁷:

$$\mu_{water} = \alpha 10^{\left(\frac{\beta}{T-\delta} \right)}, \quad (8)$$

where, $\alpha = 2.414 \times 10^{-5}$, $\beta = 247.8$, and $\delta = 140$.

Specific heat³⁶:

$$(C_p)_{water} = \exp \left(\frac{8.29041 - 0.012557T}{1 - (1.52373 \times 10^{-3})T} \right). \quad (9)$$

The properties of the nanofluid are estimated using³⁵⁻³⁷:

$$\rho_{eff} = (1 - \varnothing) \rho_{water} + \varnothing \rho_s, \quad (10)$$

$$c_{p,eff} = \frac{(1 - \varnothing)(\rho c_p)_{water} + \varnothing(\rho c_p)_s}{(1 - \varnothing)\rho_{water} + \varnothing \rho_s}, \quad (11)$$

For the nanofluid viscosity, the correlation suggested by Maiga et al.⁶ is employed.

$$\mu_{eff} = (1 + 7.3\phi + 123\phi^2) \mu_{water}, \quad (12)$$

The thermal conductivity could be also obtained as Chon et al.³⁷ recommended:

$$k_{eff}/k_{water} = 1 + 64.7(\phi)^{0.7460} \left(\frac{d_{water}}{d_s} \right)^{0.3690} \left(\frac{k_{water}}{k_s} \right)^{0.7476} Pr^{0.9955} Re_{np}^{1.2321}, \quad (13)$$

	Study condition	Nu
Present study	Re = 10.846×10^3 0.08 vol.% Al ₂ O ₃ /water	89.37
Experimental study ³⁸	Re = 9.65×10^3 0.135 vol.% Al ₂ O ₃ /water	74.10
	Re = 10.90×10^3 0.067 vol.% Al ₂ O ₃ /water	84.85

Table 1. CFD verification test.

$$\begin{cases} 294 < T < 344 \\ 11nm < ds < 150nm, \end{cases}$$

$$Re_{np} = \frac{\rho_{water}BT}{3\pi\mu_{water}^2\gamma}, \quad (14)$$

where $\gamma = 0.17$ nm is defined as the mean free path between water molecules and B is the constant of Boltzmann. This correlation is recommended for Al₂O₃/water nanofluid and the temperature of 294 K to 344 K.

Grid dependency test. The meshing process was carried out using the design modeller tool existing in ANSYS. Two different mesh densities were selected for testing the independence of the models from the mesh size (i.e. 1,074,537 nodes and 6,751,125 nodes). The temperatures obtaining from both mesh sizes were the same. So, all CFD simulations have been done based on the first mesh density.

CFD validation. For verification of the CFD results, the average Nusselt number of the dilute Al₂O₃/water nanofluid (i.e. 0.08 volume fraction) of this simulation is compared with the measured results taken from the literature. Table 1 illustrates the sample results of both studies with an acceptable agreement.

GAS (genetic algorithms). Essentially, genetic algorithms are for searching in terms of natural genetics and nature's mechanics (such as natural selection, the fittest survival)^{39,40}. Indeed, GAS analyzes the encodings of the parameters rather than the real ones. These factor sets are decreased to some signs from an arbitrary, yet operative alphabet and the solutions are assessed in terms of the given symbol structures. A population of solution structures is maintained by GAS through the procedure; hence, they are not restricted by selecting the primary single point solution guesses. Only the encoding techniques and objective function should be defined within the programmer in the case of GAS^{39–41}.

Fuzzy inference system (FIS). FIS is based on training process, and is capable to utilize other algorithms as a trainer for example using ant colont optimization algorithm called ACOFIS and using artificial neural network as a trainer called ANFIS³⁰. There are three types of fuzzy sets proposed and implemented by Takagi and Sugeno⁴² where the rth rule function is stated as^{42,43}:

$$w_r = \mu_{Ar}(\theta)\mu_{Br}(r)\mu_{Cr}(z)\mu_{Dr}(Tin)\mu_{Er}(TKE), \quad (15)$$

where w_r represents the weight of each rule in the fuzzy structure, and μ indicates the membership functions (MF) incoming signals based on each inputs, e.g. angle (θ), radius (r), z-direction (z), inlet temperature (T_{in}), and turbulence kinetic energy (TKE) in this work.

The amount of firing strength is determined for each rule^{42,44}:

$$\bar{w}_r = \frac{w_r}{\sum (w_r)}, \quad (16)$$

where \bar{w}_r is known as normalized firing strengths. The function of a consequence if-then rule presented by Takagi and Sugeno is applied⁴².

Consequently, the function of the nodes is^{42,45,29}:

$$\bar{w}_r f_r = \bar{w}_r (o_r\theta + p_r r + q_r z + r_r Tin + s_r TKE + u_r), \quad (17)$$

where $o_r, p_r, q_r, r_r, s_r,$ and u_r show the parameters of the if-then rules and are termed consequent parameters. We have developed and implemented this approach in our previous works for simulation of physical systems^{21,24,45–49,29}.

Results and discussion

After finding the intelligence, the implicit function between the flow variables could be developed. This study is intended to show how the genetic algorithm with a fuzzy interface system (GAFIS) can be used for this purpose. The turbulent nanofluid flow of Al₂O₃/water in a circular tube is the case for CFD modeling. The single-phase theory (i.e. homogeneous distribution of nanoparticles in the based fluid) is considered for the nanofluid

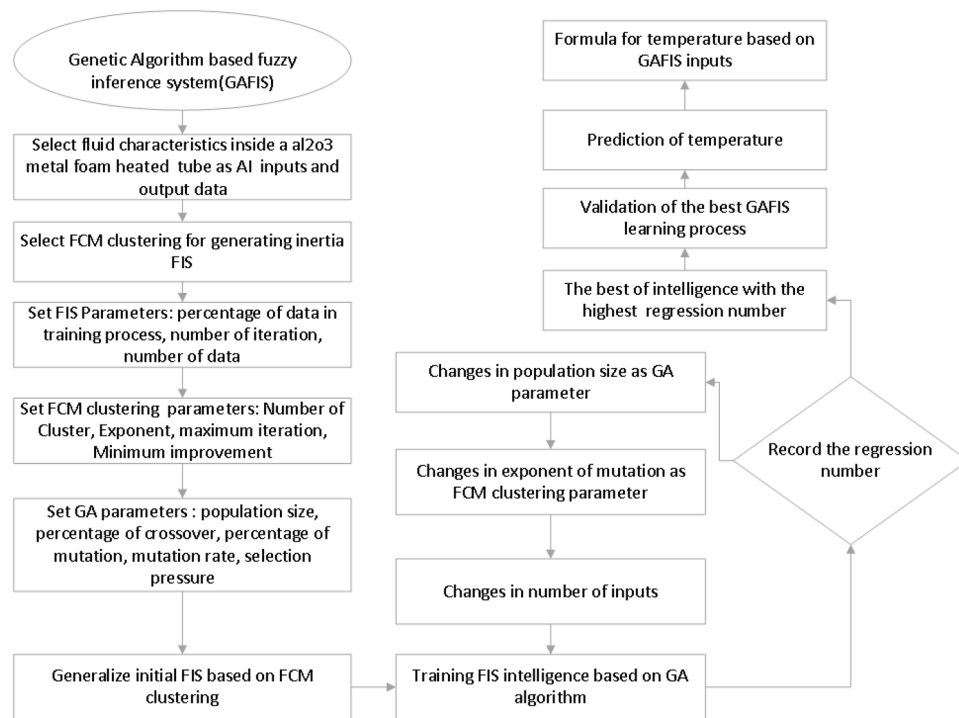


Figure 1. Flowchart of GAFIS method.

modeling. Figure 1 illustrates all steps for setup and prediction of the target variables of the GAFIS. The GAFIS trains the inlet temperature, the cylindrical coordinates (i.e. r , θ , and z) of the nodes in the pipe domain and their corresponding turbulent kinetic energy (TKE), as inputs, and the temperature of the nodes, as the output. The number of inputs increases step by step until the best intelligence condition is met³².

The fuzzy C-means clustering (FCM) is selected for generating inertia FIS in this simulation case study²⁹. For setting FIS parameters, the number of data, the number of iterations, and the percentage of data in the training are determined equal to 24,164, 150, and 75% respectively. As the FCM parameter, 10 clusters are considered for each input. Different numbers of exponents (i.e. 2, 3, 4, and 5), as the FCM parameter, are checked during the modeling so that the best intelligence is derived. The population size as one of the genetic algorithm parameters are also checked for the values of 5, 10, 20, and 30 until the best intelligence is found. After the definition of all parameters, a genetic algorithm based on FIS begins the training of the data. The temperature of the nanofluid predicted by the GAFIS is compared by that predicted by the CFD. The more regression number, the best intelligence is achieved.

Figure 2 shows the domain of the nodes learned by the GAFIS. According to Fig. 2, the r is between 0 to 5 (mm), the θ is between ± 2 (rad), and the z is between 0.1 to 0.9 (m). The cross-section view of the nodes is also shown in Fig. 3.

Figure 4 shows the regression number changes by adding the inputs. The highest regression number (i.e. 0.97) is obtained by considering all 5 inputs (i.e. r , θ , z , inlet temperature, and TKE). It should be noted that by adding the turbulent kinetic energy as the fifth input the regression value increases from 0.95 to 0.98. This means that considering the turbulent kinetic energy the GAFIS reaches a higher level of intelligence by distinguishing the more difference between the learned data.

According to Figs. 5 and 6, the highest regression number (i.e. 0.979) is related to the exponent of 3 and the population size of 30. So, the best intelligence can be found for 5 inputs, the exponent of 3, and the population size of 30.

Schematic diagram of the GAFIS structure is shown in Fig. 7. The number cluster for each input, the number of rules, and the number of membership functions of the output all are equal to 10. The Gaussian function is considered for membership function in this case. The shape of the Gaussian function is schematically shown on the left side of Fig. 7. The temperatures of the CFD prediction are compared with those of the GAFIS. A high compatibility exists between both predictions as depicted in Fig. 8. Figure 9 illustrates the temperature distribution of the nodes for different inlet temperatures versus the turbulent kinetic energy and the dimensionless positions of the nodes. As expected, the TKE is zero on the wall. This is because there is not any slip velocity on the wall. The TKE is maximum in the vicinity of the wall and within the hydrodynamic boundary layer. As getting closer to the pipe centerline and far from the wall, the TKE decreases.

Finally, a general formula is developed to determine the nanofluid temperature in domain depending on the inputs. According to Eq. (18), once the optimum intelligence of the model is established, the consequent factors and the parameters of the Gaussian function can be found³². Table 2 shows the general equation of the Gaussian

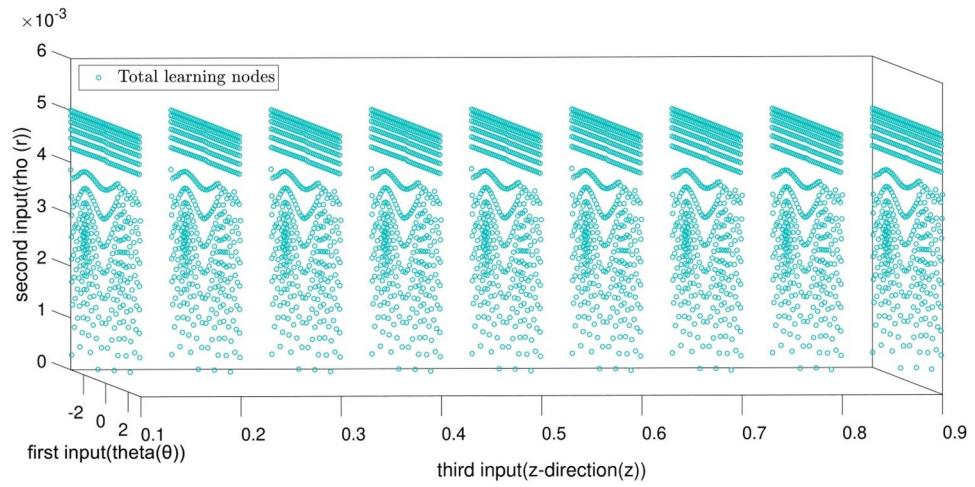


Figure 2. Learning data which is CFD output.

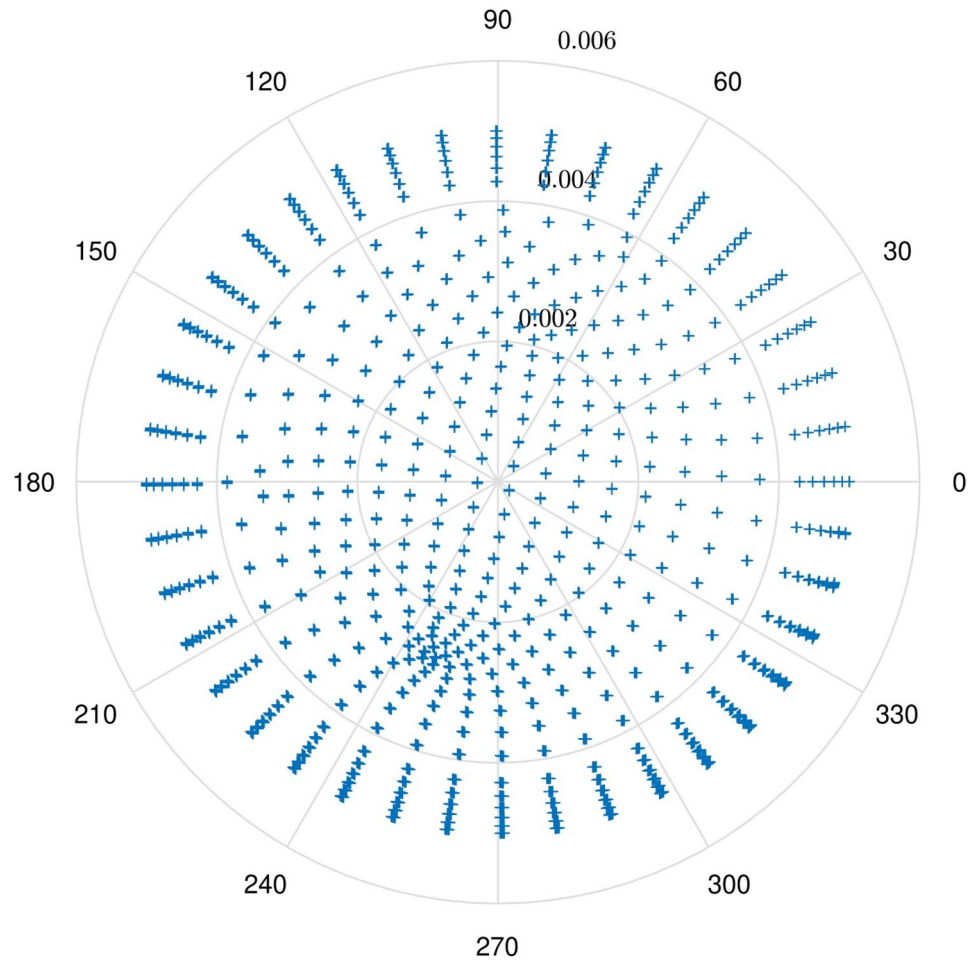


Figure 3. The cross-section of learning nodes.

function and its parameters (i.e. C , and σ). Table 3 indicates the Gaussian function parameters for each cluster in each input. So, there are 10 sets of data, based on 10 clusters, for each of 5 inputs. Table 4 also shows 10 sets of the consequent parameters (i.e. o_m , p_m , q_m , r_m , s_m , and u_m) for all 10 clusters. In this way, the temperature of

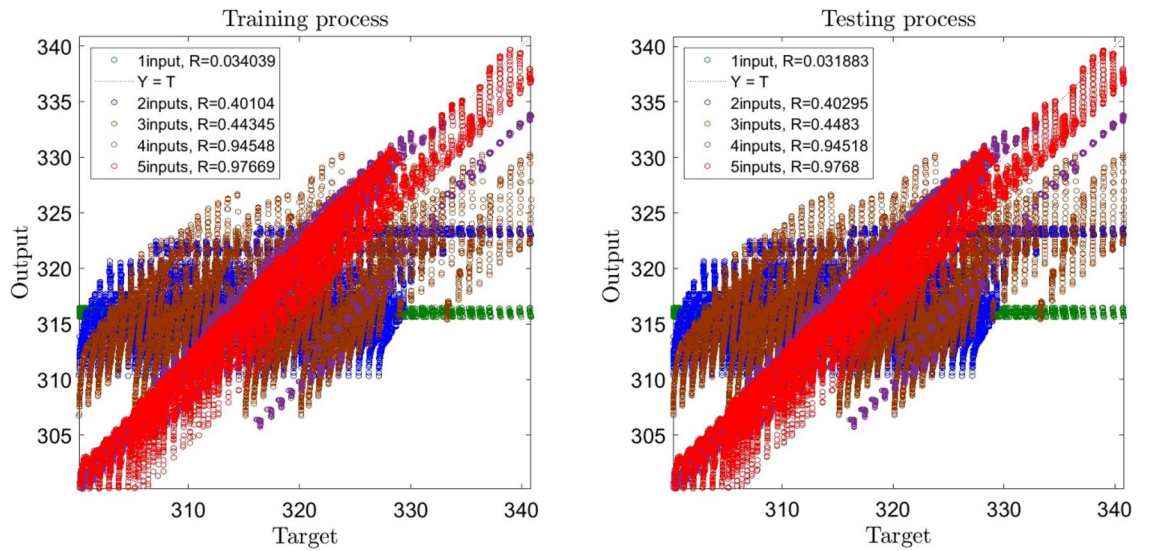


Figure 4. Learning process with changes in number of inputs from one to five.

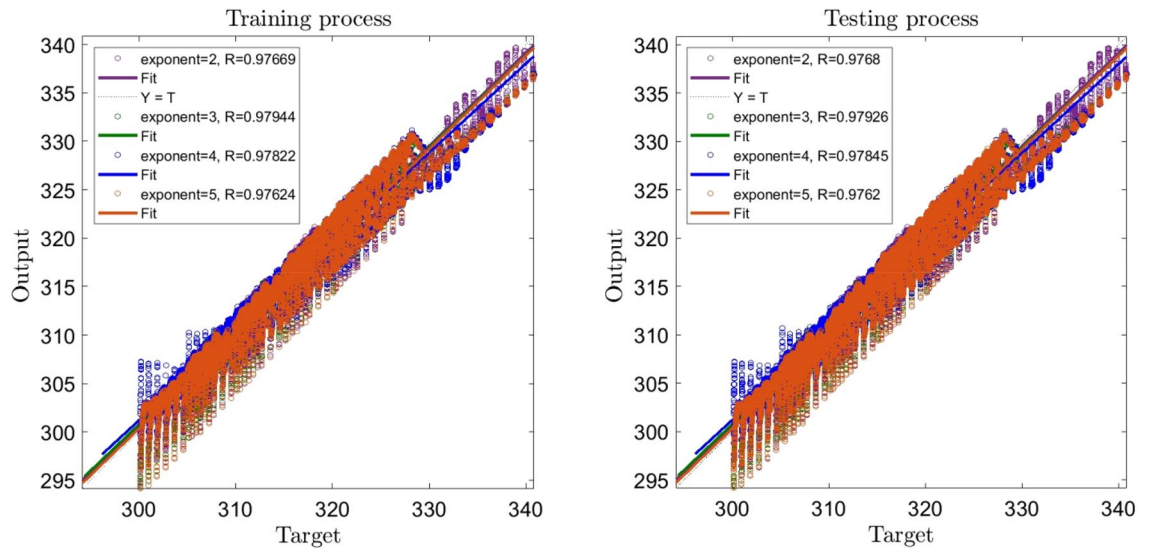


Figure 5. Learning process with changes in exponent as FCM clustering parameter (2,3,4,5).

the nanofluid can be found relating to any values of the inlet temperature and anywhere in the domain without CFD modeling.

$$temperature = \frac{\sum_{i=1}^{10} \sum_{j=1}^{10} \sum_{k=1}^{10} \sum_{l=1}^{10} \sum_{n=1}^{10} (\mu_{1i} \times \mu_{2j} \times \mu_{3k} \times \mu_{4l} \times \mu_{5n}) \times (o_m \theta \times p_m r \times q_m z \times r_m T_{inlet} \times s_m TKE \times u_m)}{\sum_{i=1}^{10} \sum_{j=1}^{10} \sum_{k=1}^{10} \sum_{l=1}^{10} \sum_{n=1}^{10} (\mu_{1i} \times \mu_{2j} \times \mu_{3k} \times \mu_{4l} \times \mu_{5n})} \tag{18}$$

In which:

$$\mu_{1i} = e^{-\frac{(x - c_j)^2}{(2\sigma^2)}}, \mu_{2j} = e^{-\frac{(x - c_j)^2}{(2\sigma^2)}}, \mu_{3k} = e^{-\frac{(x - c_j)^2}{(2\sigma^2)}}, \mu_{4l} = e^{-\frac{(x - c_j)^2}{(2\sigma^2)}} \text{ and } \mu_{5n} = e^{-\frac{(x - c_j)^2}{(2\sigma^2)}} \tag{19}$$

Conclusion

This work was aimed to provide a facile approach to connect the fluid flow characteristics resulted from the computational fluid dynamic (CFD) predictions. The CFD is able to predict all hydro-thermal parameters of fluid flows. But there is no way to find the connections such parameters with each other using the CFD. Machine

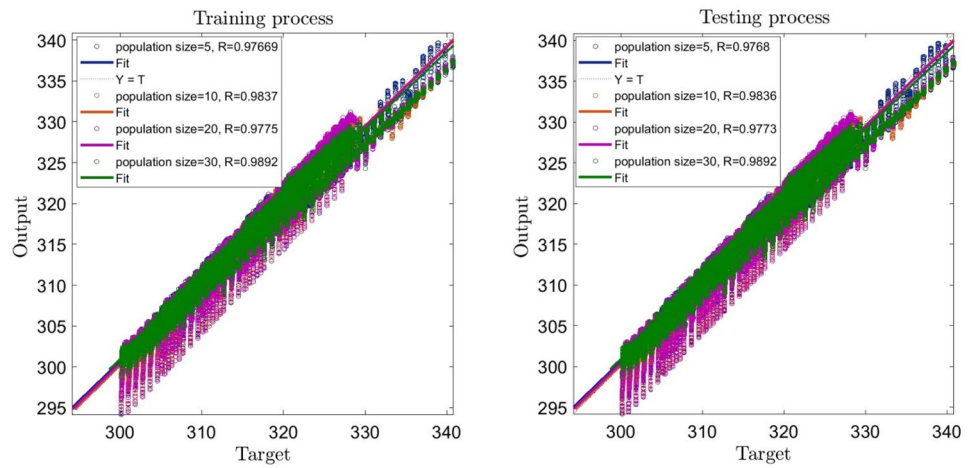


Figure 6. Learning process with changes in population size as GA parameter (5,10,20,30).

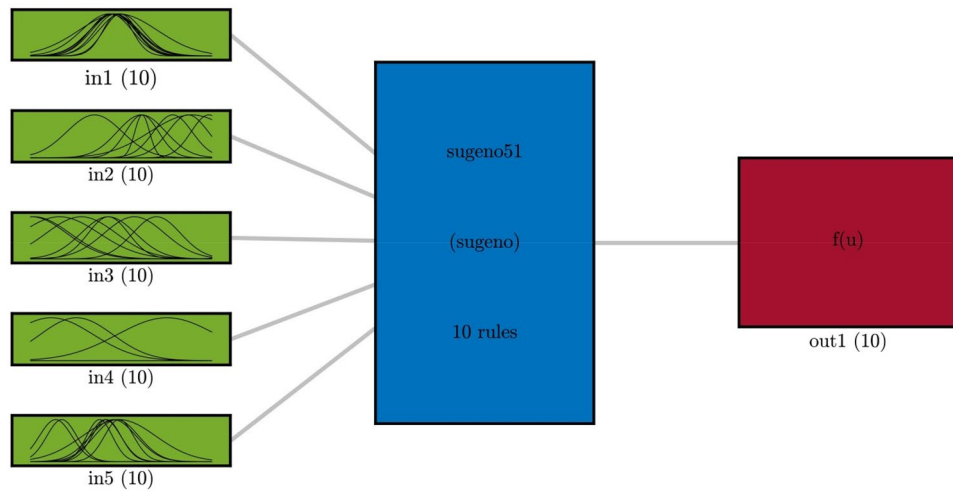
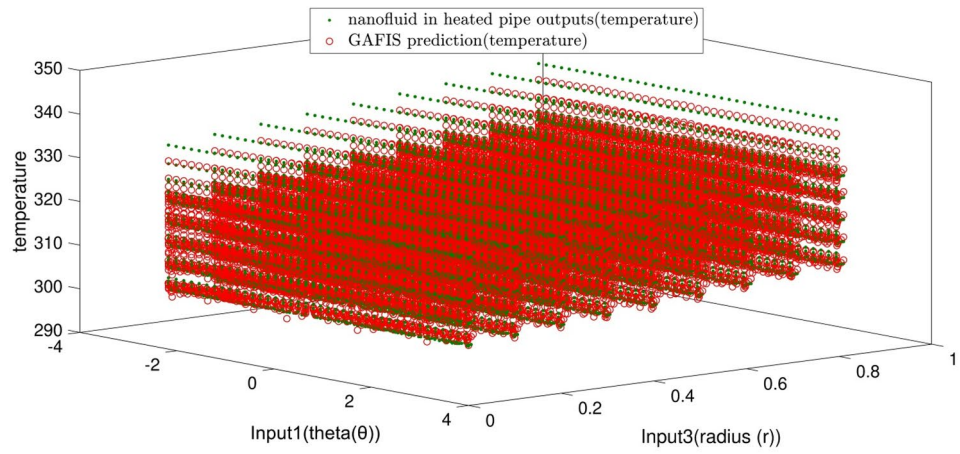
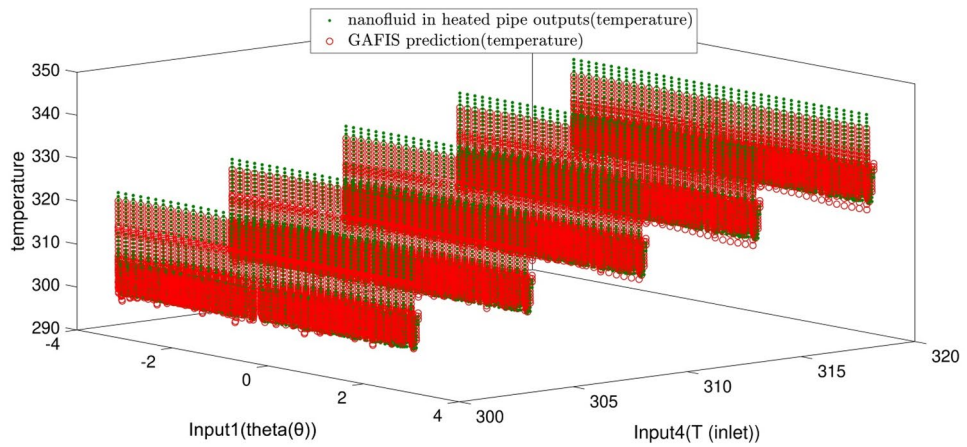


Figure 7. GAFIS structure in the best result of learning.

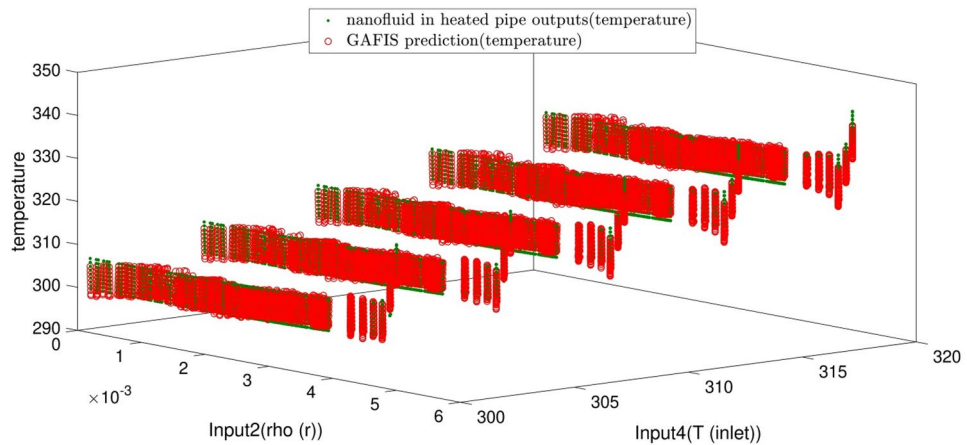
learning by the artificial intelligence (AI) algorithm could intelligently record the data patterns. However, such a pattern record does not exist for the CFD data. For this purpose, the simulation of convection of Al_2O_3 /water nanofluid in a tube was simulated at the turbulence flow regime. The artificial intelligence of the genetic algorithm with the fuzzy interface system was used for integration with the CFD. The cylindrical coordinates (i.e. r , θ , and z) of the CFD nodes, the inlet temperature, and the turbulent kinetic energy (TKE) were learned as inputs to predict the temperature of the nodes in the system of interest. Different input numbers, population sizes, and exponents were used in order to get the best intelligence of GAFIS. The results discovered that the best intelligence of GAFIS was obtained for 5 inputs, the population size of 30, and the exponent of 3. Adding the turbulent kinetic energy as the fifth input the regression value increases from 0.95 to 0.98. This means that considering the turbulent kinetic energy the GAFIS reaches a higher level of intelligence by distinguishing the more difference between the learned data. At the best intelligence, the predicted temperatures by the GAFIS were the same as those predicted by the CFD. The regression number for this condition was around 0.98. Then, using the GAFIS, a correlation was developed to relate the temperature of the node to the inputs (i.e. cylindrical coordinates, inlet temperature, and TKE).



a Prediction of temperature and its validation with CFD results using inputs 1 and 3.



b Prediction of temperature and its validation with CFD results using inputs 1 and 4.



c Prediction of temperature and its validation with CFD results using inputs 2 and 4.

Figure 8. (a) Prediction of temperature and its validation with CFD results using inputs 1 and 3. (b) Prediction of temperature and its validation with CFD results using inputs 1 and 4. (c) Prediction of temperature and its validation with CFD results using inputs 2 and 4.

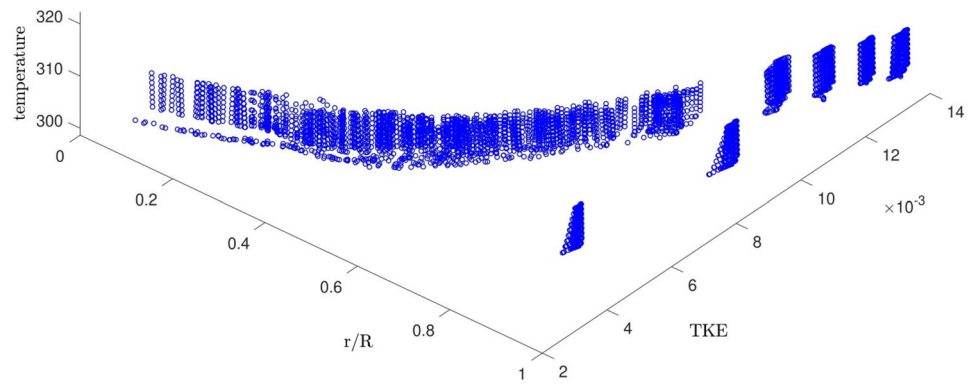


Figure 9. The temperature distribution for different inlet temperatures versus the turbulent kinetic energy and the dimensionless positions of the nodes.

Membership function	Equation
Gaussian	$e^{-\frac{(x-c)^2}{2\sigma^2}}$

Table 2. Gaussian membership function equation in GAFIS learning process.

Number of cluster	Type of MFs	σ	C	Number of cluster	Type of MFs	σ	C
'in1cluster1'	'gaussmf'	0.826635429	-0.257424169	'in3cluster6'	'gaussmf'	0.15393271	0.106704257
'in1cluster2'	'gaussmf'	0.576086004	-0.028883971	'in3cluster7'	'gaussmf'	0.111842544	-0.858703931
'in1cluster3'	'gaussmf'	0.757543057	-0.263228836	'in3cluster8'	'gaussmf'	0.174190572	0.229131334
'in1cluster4'	'gaussmf'	0.69040043	-0.206462468	'in3cluster9'	'gaussmf'	0.105266664	0.655767376
'in1cluster5'	'gaussmf'	0.85294523	-0.239048447	'in3cluster10'	'gaussmf'	0.084140256	1.133442934
'in1cluster6'	'gaussmf'	0.730274295	-0.354283281	'in4cluster1'	'gaussmf'	1.618098253	379.5749903
'in1cluster7'	'gaussmf'	1.358895591	-0.103305891	'in4cluster2'	'gaussmf'	4.009478411	305.0873344
'in1cluster8'	'gaussmf'	0.958817478	-0.414412627	'in4cluster3'	'gaussmf'	3.707930813	112.4063766
'in1cluster9'	'gaussmf'	0.501674052	-0.122800932	'in4cluster4'	'gaussmf'	5.965432157	160.8270081
'in1cluster10'	'gaussmf'	-0.760020363	-0.017918213	'in4cluster5'	'gaussmf'	4.629180724	302.3176448
'in2cluster1'	'gaussmf'	0.000642441	0.003135137	'in4cluster6'	'gaussmf'	2.530182626	89.77626929
'in2cluster2'	'gaussmf'	0.000509462	0.003960464	'in4cluster7'	'gaussmf'	9.846234379	375.0116229
'in2cluster3'	'gaussmf'	0.000532355	0.004366219	'in4cluster8'	'gaussmf'	5.479436302	315.0356584
'in2cluster4'	'gaussmf'	-0.000434711	0.003151819	'in4cluster9'	'gaussmf'	2.951138918	333.0374101
'in2cluster5'	'gaussmf'	0.000668226	-0.001951237	'in4cluster10'	'gaussmf'	2.872943793	250.0895913
'in2cluster6'	'gaussmf'	0.001099873	0.004459562	'in5cluster1'	'gaussmf'	0.001163133	0.00398334
'in2cluster7'	'gaussmf'	0.000731798	0.001894067	'in5cluster2'	'gaussmf'	0.001066247	0.004421655
'in2cluster8'	'gaussmf'	-0.000194298	0.003152282	'in5cluster3'	'gaussmf'	0.00103551	0.007600883
'in2cluster9'	'gaussmf'	7.53E-05	-0.000877803	'in5cluster4'	'gaussmf'	0.000487411	0.025364583
'in2cluster10'	'gaussmf'	0.000465181	0.004910869	'in5cluster5'	'gaussmf'	0.001637584	0.008089513
'in3cluster1'	'gaussmf'	0.154370243	0.324098633	'in5cluster6'	'gaussmf'	0.001580118	0.008324729
'in3cluster2'	'gaussmf'	0.08881652	0.443553946	'in5cluster7'	'gaussmf'	0.001041173	0.00849897
'in3cluster3'	'gaussmf'	0.133380146	0.558057507	'in5cluster8'	'gaussmf'	0.000919726	0.007106961
'in3cluster4'	'gaussmf'	-0.119917998	0.44296301	'in5cluster9'	'gaussmf'	0.002619051	0.008503345
'in3cluster5'	'gaussmf'	0.158536818	0.116304464	'in5cluster10'	'gaussmf'	0.001112753	0.007515792

Table 3. Inputs membership functions parameters in GAFIS intelligence learning process.

	Output MFs	Output MFs type	o	p	q	r	s	u
1	'out1cluster1'	'linear'	0.078996019	2357.527744	10.09732893	0.947178031	- 778.9879676	9.56412065
2	'out1cluster2'	'linear'	0.079820308	4281.41413	9.180047255	0.954597364	- 1116.136518	9.56412065
3	'out1cluster3'	'linear'	0.057378996	4585.748672	8.884517906	0.233957643	- 1114.194728	2.684024609
4	'out1cluster4'	'linear'	0.107061914	3411.50903	10.92249369	1.412137104	- 1114.194728	5.112260621
5	'out1cluster5'	'linear'	0.080157462	3014.783586	9.180077769	0.954597364	- 1116.270466	14.27288647
6	'out1cluster6'	'linear'	0.080157462	4181.356389	11.6245228	0.605227692	- 911.4273206	10.47376635
7	'out1cluster7'	'linear'	0.080157462	4556.321232	7.710165876	0.950779527	- 806.6211222	22.62104405
8	'out1cluster8'	'linear'	2.31E- 01	4191.570094	7.462891624	0.954597364	- 1171.080269	9.56412065
9	'out1cluster9'	'linear'	0.082528737	4190.388858	8.902586343	0.954597364	- 917.8175631	9.56412065
10	'out1cluster10'	'linear'	0.07993579	2582.906758	7.853218312	- 0.42716382	- 1261.150587	9.562570627

Table 4. GAFIS method consequent parameters for predicting temperature.

Received: 9 September 2020; Accepted: 17 December 2020

Published online: 14 January 2021

References

1. Pryazhnikov, M., Minakov, A., Rudyak, V. Y. & Guzei, D. Thermal conductivity measurements of nanofluids. *Int. J. Heat Mass Transf.* **104**, 1275–1282 (2017).
2. Alawi, O. A., Sidik, N. A. C., Xian, H. W., Kean, T. H. & Kazi, S. N. Thermal conductivity and viscosity models of metallic oxides nanofluids. *Int. J. Heat Mass Transf.* **116**, 1314–1325 (2018).
3. Raja, R. A., Sunil, J. & Maheswaran, R. Estimation of thermo-physical properties of nanofluids using theoretical correlations. *Int. J. Appl. Eng. Res.* **13**, 7950–7953 (2018).
4. Phanindra, Y., Kumar, S. & Pugazhendhi, S. Experimental investigation on Al₂O₃ & Cu/Oil hybrid nano fluid using concentric tube heat exchanger. *Mater. Today Proc.* **5**, 12142–12150 (2018).
5. Choi, S. U. & Eastman, J. A. *Enhancing Thermal Conductivity of Fluids with Nanoparticles* (Argonne National Lab, United States, 1995).
6. Maïga, S. E. B., Nguyen, C. T., Galanis, N. & Roy, G. Heat transfer behaviours of nanofluids in a uniformly heated tube. *Superlattices Microstruct.* **35**, 543–557 (2004).
7. Behroyan, I., Ganesan, P., He, S. & Sivasankaran, S. Turbulent forced convection of Cu–water nanofluid: CFD model comparison. *Int. Commun. Heat Mass Transfer* **67**, 163–172 (2015).
8. Behroyan, I., Vanaki, S. M., Ganesan, P. & Saidur, R. A comprehensive comparison of various CFD models for convective heat transfer of Al₂O₃ nanofluid inside a heated tube. *Int. Commun. Heat Mass Transfer* **70**, 27–37 (2016).
9. Bahmani, M. H. *et al.* Investigation of turbulent heat transfer and nanofluid flow in a double pipe heat exchanger. *Adv. Powder Technol.* **29**, 273–282 (2018).
10. Bianco, V., Marchitto, A., Scarpa, F. & Tagliafico, L. A. Numerical investigation on the forced laminar convection heat transfer of Al₂O₃-water nanofluid within a three-dimensional asymmetric heated channel. *Int. J. Numer. Methods Heat Fluid Flow* (2019).
11. Benkhedda, M., Boufendi, T., Tayebi, T. & Chamkha, A. J. Convective heat transfer performance of hybrid nanofluid in a horizontal pipe considering nanoparticles shapes effect. *J. Therm. Anal. Calorim.* **140**, 411–425 (2020).
12. Sharma, K. V. *et al.* Influence of nanofluid properties on turbulent forced convection heat transfer in different base liquids. *Math. Methods Appl. Sci.* (2020).
13. Zainon, S. & Azmi, W. in *IOP Conference Series: Materials Science and Engineering*. 012051 (IOP Publishing).
14. Kumar, S. L. State of the art-intense review on artificial intelligence systems application in process planning and manufacturing. *Eng. Appl. Artif. Intell.* **65**, 294–329 (2017).
15. Suman, S., Khan, S., Das, S. & Chand, S. Slope stability analysis using artificial intelligence techniques. *Nat. Hazards* **84**, 727–748 (2016).
16. Halim, Z., Kalsoom, R., Bashir, S. & Abbas, G. Artificial intelligence techniques for driving safety and vehicle crash prediction. *Artif. Intell. Rev.* **46**, 351–387 (2016).
17. Saleem, M., Di Caro, G. A. & Farooq, M. Swarm intelligence based routing protocol for wireless sensor networks: Survey and future directions. *Inf. Sci.* **181**, 4597–4624 (2011).
18. Mellit, A., Kalogirou, S. A., Hontoria, L. & Shaari, S. Artificial intelligence techniques for sizing photovoltaic systems: A review. *Renew. Sustain. Energy Rev.* **13**, 406–419 (2009).
19. Mellit, A. & Kalogirou, S. A. Artificial intelligence techniques for photovoltaic applications: A review. *Prog. Energy Combust. Sci.* **34**, 574–632 (2008).
20. Aytek, A. & Alp, M. An application of artificial intelligence for rainfall-runoff modeling. *J. Earth Syst. Sci.* **117**, 145–155 (2008).
21. Babanezhad, M., Behroyan, I., Marjani, A. & Shirazian, S. Artificial intelligence simulation of suspended sediment load with different membership functions of ANFIS. *Neural Comput. Appl.* 1–15 (2020).
22. Nguyen, Q., Behroyan, I., Rezakazemi, M. & Shirazian, S. Fluid velocity prediction inside bubble column reactor using ANFIS algorithm based on CFD input data. *Arab. J. Sci. Eng.* (2020).
23. Zhou, J., Li, C., Arslan, C. A., Hasanipanah, M. & Amnieh, H. B. Performance evaluation of hybrid FFA-ANFIS and GA-ANFIS models to predict particle size distribution of a muck-pile after blasting. *Eng. Comput.* 1–10 (2019).
24. Xu, P., Babanezhad, M., Yarmand, H. & Marjani, A. Flow visualization and analysis of thermal distribution for the nanofluid by the integration of fuzzy c-means clustering ANFIS structure and CFD methods. *J. Vis.* 1–14 (2019).
25. Chin, R. J., Lai, S. H., Ibrahim, S., Jaafar, W. Z. W. & Elshafie, A. ANFIS-based model for predicting actual shear rate associated with wall slip phenomenon. *Soft Comput.* 1–11 (2019).
26. Pourtousi, M., Zeinali, M., Ganesan, P. & Sahu, J. Prediction of multiphase flow pattern inside a 3D bubble column reactor using a combination of CFD and ANFIS. *RSC Adv.* **5**, 85652–85672 (2015).
27. Pourtousi, M., Sahu, J., Ganesan, P., Shamshirband, S. & Redzwan, G. A combination of computational fluid dynamics (CFD) and adaptive neuro-fuzzy system (ANFIS) for prediction of the bubble column hydrodynamics. *Powder Technol.* **274**, 466–481 (2015).
28. Pishnamazi, M. *et al.* ANFIS grid partition framework with difference between two sigmoidal membership functions structure for validation of nanofluid flow. *Sci. Rep.* **10**, 1–11 (2020).

29. Babanezhad, M., Behroyan, I., Nakhjiri, A. T., Marjani, A., & Shirazian, A. Computational modeling of transport in porous media using an adaptive network-based fuzzy inference system. *ACS Omega* **5**(48), 30826–30835 (2020).
30. Babanezhad, M., Behroyan, I., Nakhjiri, A. T., Marjani, A., Heydarinasab, A. & Shirazian, A. Liquid temperature prediction in bubbly flow using ant colony optimization algorithm in the fuzzy inference system as a trainer. *Sci. Rep.* **10**(1) (2020).
31. Bird, R., Stewart, W. & Lightfoot, E. *Transport Phenomena* 2nd edn. (John Wiley and Sons, Inc., Hoboken, 2002).
32. Marjani, A., Babanezhad, M. & Shirazian, S. Application of adaptive network-based fuzzy inference system (ANFIS) in the numerical investigation of Cu/water nanofluid convective flow. *Case Stud. Therm. Eng.* <https://doi.org/10.1016/j.csite.2020.100793> (2020).
33. Bianco, V., Manca, O. & Nardini, S. Numerical investigation on nanofluids turbulent convection heat transfer inside a circular tube. *Int. J. Therm. Sci.* **50**, 341–349 (2011).
34. Ganesan, P., Behroyan, I., He, S., Sivasankaran, S. & Sandaran, S. C. Turbulent forced convection of Cu–water nanofluid in a heated tube: Improvement of the two-phase model. *Numer. Heat Transfer Part A: Appl.* **69**, 401–420 (2016).
35. Akbari, M., Galanis, N. & Behzadmehr, A. Comparative analysis of single and two-phase models for CFD studies of nanofluid heat transfer. *Int. J. Therm. Sci.* **50**, 1343–1354 (2011).
36. Reid, R. C. Tables on the thermophysical properties of liquids and gases. NB Vargaftik, Halsted Press, Division of John Wiley & Sons, Inc., New York, August, 1975. \$49.50, 758 pages. *Aiche J.* **21**, 1235–1235 (1975).
37. Chon, C. H., Kihm, K. D., Lee, S. P. & Choi, S. U. Empirical correlation finding the role of temperature and particle size for nanofluid (Al_2O_3) thermal conductivity enhancement. *Appl. Phys. Lett.* **87**, 153107 (2005).
38. Fotukian, S. & Esfahany, M. N. Experimental investigation of turbulent convective heat transfer of dilute $\gamma\text{-Al}_2\text{O}_3$ /water nanofluid inside a circular tube. *Int. J. Heat Fluid Flow* **31**, 606–612 (2010).
39. Goldberg, D. E. Genetic algorithms in search. *Optim. Mach. Learn.* (1989).
40. Ettaouil, M. & Ghanou, Y. Neural architectures optimization and Genetic algorithms. *Wseas Trans. Comput.* **8**, 526–537 (2009).
41. Walters, D. C. & Sheble, G. B. Genetic algorithm solution of economic dispatch with valve point loading. *IEEE Trans. Power Syst.* **8**, 1325–1332. <https://doi.org/10.1109/59.260861> (1993).
42. Takagi, T. & Sugeno, M. Fuzzy identification of systems and its applications to modeling and control. *IEEE Trans. Syst. Man Cybern.* 116–132 (1985).
43. Babanezhad, M., Taghvaei Nakhjiri, A., Rezakazemi, M. & Shirazian, S. Developing intelligent algorithm as a machine learning overview over the big data generated by Euler–Euler method to simulate bubble column reactor hydrodynamics. *ACS Omega* (2020).
44. Nguyen, Q., Babanezhad, M., Taghvaei Nakhjiri, A., Rezakazemi, M. & Shirazian, S. Prediction of thermal distribution and fluid flow in the domain with multi-solid structures using cubic-interpolated pseudo-particle model. *PLoS ONE* **15**, e0233850 (2020).
45. Babanezhad, M. *et al.* Prediction of turbulence eddy dissipation of water flow in a heated metal foam tube. *Sci. Rep.* **10**, 1–12 (2020).
46. Babanezhad, M., Nakhjiri, A. T., Marjani, A., Rezakazemi, M. & Shirazian, S. Evaluation of product of two sigmoidal membership functions (psigmf) as an ANFIS membership function for prediction of nanofluid temperature. *Sci. Rep.* **10**, 22337 (2020).
47. Babanezhad, M., Pishnamazi, M., Marjani, A. & Shirazian, S. Bubbly flow prediction with randomized neural cells artificial learning and fuzzy systems based on k- ϵ turbulence and Eulerian model data set. *Sci. Rep.* **10**, 1–12 (2020).
48. Babanezhad, M., Rezakazemi, M., Hajilary, N. & Shirazian, S. Liquid-phase chemical reactors: Development of 3D hybrid model based on CFD-adaptive network-based fuzzy inference system. *Can. J. Chem. Eng.* <https://doi.org/10.1002/cjce.23378> (2018).
49. Tian, E., Babanezhad, M., Rezakazemi, M. & Shirazian, S. Simulation of a bubble-column reactor by three-dimensional CFD: Multidimension- and function-adaptive network-based fuzzy inference system. *Int. J. Fuzzy Syst.* **22**, 477–490. <https://doi.org/10.1007/s40815-019-00741-8> (2020).

Acknowledgements

S. Shirazian gratefully acknowledges the supports by the Government of the Russian Federation (Act 211, contract 02.A03.21.0011) and the Ministry of Science and Higher Education of the Russian Federation (grant FENU-2020-0019).

Author contributions

M.B.: Writing-draft, Simulations, Conceptualization. I.B.: Modeling, Writing-draft. A.T.N.: Analysis, Software. M.R.: Writing-review, Revision, Validation. A.M.: Supervision, Project administration. S.S.: Supervision, Modeling, Validation.

Competing interests

The authors declare no competing interests.

Additional information

Correspondence and requests for materials should be addressed to A.M.

Reprints and permissions information is available at www.nature.com/reprints.

Publisher's note Springer Nature remains neutral with regard to jurisdictional claims in published maps and institutional affiliations.



Open Access This article is licensed under a Creative Commons Attribution 4.0 International License, which permits use, sharing, adaptation, distribution and reproduction in any medium or format, as long as you give appropriate credit to the original author(s) and the source, provide a link to the Creative Commons licence, and indicate if changes were made. The images or other third party material in this article are included in the article's Creative Commons licence, unless indicated otherwise in a credit line to the material. If material is not included in the article's Creative Commons licence and your intended use is not permitted by statutory regulation or exceeds the permitted use, you will need to obtain permission directly from the copyright holder. To view a copy of this licence, visit <http://creativecommons.org/licenses/by/4.0/>.

© The Author(s) 2021